ISSN: 2447-3359

REVISTA DE GEOCIÊNCIAS DO NORDESTE

Northeast Geosciences Journal

v. 10, nº 2 (2024)

https://doi.org/10.21680/2447-3359.2024v10n2ID36390

Mapping of impermeable surfaces in Western Bahia using Machine Learning Algorithm

Mapeamento de superfícies impermeáveis no Oeste da Bahia utilizando algoritmo de Aprendizado de Máquina

Gustavo Gonçalves de Souza[1]; Elvis Bergue Mariz Moreira[2]; Admilson da Penha Pacheco[3]; Fabio Corrêa Alves[4]; Henrique dos Santos Ferreira[5]

[1] Federal University of Western Bahia, Center for Exact Sciences and Technologies, Barreiras /BA, Brasil. Email: gustavo.goncalves@ufob.edu.br
ORCID: https://orcid.org/0009-0004-3732-2510

[2] Federal University of Western Bahia, Humanities Center, Barreiras/BA, Brasil. Email: elvis.moreira@ufob.edu.br
ORCID: https://orcid.org/0000-0001-6732-3005

[3] Federal University of Pernambuco, Department of Cartographic Engineering, Recife/PE, Brasil. Email: pacheco3p@gmail.com
ORCID: https://orcid.org/0000-0002-3635-827X

[4] Federal University of Western Bahia, Humanities Center, Barreiras/BA, Brasil. Email: fabio.alves@ufob.edu.br
ORCID: https://orcid.org/0000-0002-2941-8393

[5] Data and Knowledge Integration Center for Health - CIDACS, Salvador/BA, Brasil. Email: ferreira.hds@hotmail.com
ORCID: https://orcid.org/0000-0003-3134-4984

Abstract: Urban impermeable surface is a relevant parameter in climate, environmental change and sustainability, and is fundamental in detecting urban environmental quality. Mapping makes it possible to measure the level of a city's urbanization and can provide indications of social, economic and environmental impacts. However, few studies have used high spatial resolution satellite images to analyze cities with significant urban growth in recent years, especially in western Bahia. The aim of this study was to map the impermeable areas of the city of Barreiras-BA using images from the CBERS-4A satellite and the Random Forest (RF) machine learning algorithm. The visible spectral bands dated from 13/06/2023 were used for color composition and image fusion to obtain 2m pixels. The fused image was classified using RF and validated using the confusion matrix, global accuracy and Kappa index. The results showed that in the city of Barreiras 41.11% correspond to impermeable surfaces. The accuracy metrics found were 0.79 for the Kappa index and 91.7% for Global Accuracy. The results found can be used as a basis for future research into mapping land use and occupation in urban perimeters.

Keywords: Remote sensing; Urbanization; CBERS–4A.

Resumo: A superfície impermeável urbana é um parâmetro relevante nas mudanças climáticas, ambientais e na sustentabilidade, sendo fundamental na detecção da qualidade ambiental urbana. O mapeamento possibilita mensurar o nível de urbanização que uma cidade se encontra, podendo gerar indicativos de impactos sociais, econômicos e ambientais. Porém, poucos estudos aplicaram imagens de satélite de alta resolução espacial para a análise de cidades com significativo crescimento urbano nos últimos anos, sobretudo no oeste baiano. O objetivo deste trabalho consistiu em mapear as áreas impermeáveis da cidade de Barreiras–BA através de imagens do satélite CBERS–4A e o algoritmo de aprendizado de máquina Random Forest (RF). Utilizou–se as bandas espectrais do visível na data 13/06/2023 para a realização da composição colorida e fusão de imagens na obtenção dos *pixel*s com 2m. A imagem fusionada foi classificada com o RF e validada através da matriz de confusão, acurácia global e índice Kappa. Os resultados mostraram que na cidade de Barreiras 41,11% correspondem às superfícies impermeáveis. As métricas de exatidão encontradas foram 0,79 para o Índice Kappa, e 91,7% de Acurácia Global. Os resultados encontrados poderão ser base para futuras pesquisas sobre mapeamento do uso e ocupação do solo em perímetros urbanos.

Palavras–chave: Sensoriamento remoto; Urbanização; CBERS–4A.

Received: 22/05/2024; Accepted: 05/07/2024; Published: 12/08/2024.

1. Introduction

Since the second industrial revolution at the end of the 19th century, the world has experienced rapid urbanization at unprecedented rates that will continue in the future decades (LI et al., 2020; UNO, 2018). Rapid urbanization brings social and economic benefits as well as serious deterioration of the environment and social issues, such as air and water pollution, biodiversity loss, the urban heat island effect, runoff issues, economic and social inequality (ZHANG et al., 2021; LI et al. 2014). In this context, an impervious surface (IS) is defined by man-made features in which water cannot infiltrate, such as building roofs, driveways and parking areas (LI et al., 2020). Together with the ISs, the urbanization process contributes to changes in urban spatial structures and land surface properties (ZHU, et al., 2022). These changes occur due to the conversion of natural land surfaces into urban impervious surfaces (UIS) (SHAO, et al., 2024). IS refers to a land surface paved with impermeable or low-permeability materials within the boundaries of urban development, usually including buildings, structures, impermeable roads, paved streets, squares, parking lots, among others (CAI et al., 2022; SHAO et al., 2024).

The IS areas and the green spaces (GS), two main components of the urban environment, are fundamental in detecting urban environmental quality and addressing issues of global environmental change (KUANG et al., 2021). ISs, which represent the most common land cover in urban areas, not only provide convenience to the city, but also exert significant negative environmental impacts, affecting the carrying capacity of the ecological environment of urban agglomerations. Thus, monitoring spatially and temporally urban contexts is a crucial point for urban planning and management (ZHANG et al., 2021).

The increase in UISs has been modifying the ecological balance in metropolitan areas, impacting hydrological regimes and leading to the reduction of adjacent permeable spaces (PAREKH et al., 2021). The change from natural or semi-natural surfaces to impermeable surfaces impacts the radiation balance at the earth's interface, resulting in an increase in local surface temperature and air temperatures (KOTARBA, et al., 2016). In addition, the increasing amount of impervious surfaces can also disrupt groundwater recharge and increase the risk of flooding, as evidenced in various urban contexts (SU et al., 2022).

Remote sensing has been widely used to detect impervious surfaces (PAREKH et al., 2021). In particular, the use of freely available optical remote sensing imagery with global coverage and short revisit cycles becomes useful in applications aiming to inform sustainable urban development (SAAH et al., 2019). In the last decade, data from new multispectral and multitemporal orbital sensors with fine spatial resolutions have emerged as essential alternatives for estimating aspects such as vegetation cover, forest degradation and urban sprawl (NAIKOO et al., 2020). Remote sensing techniques have been widely applied to analyze spatio-temporal urban compositions over large geographical areas and at relatively low costs (ZHANG et al., 2021). Recent studies have focused on monitoring impervious surfaces using a wide range remote sensing data (NJOKU; TENENBAUM, 2022; OLIVATTO; INGUAGGIATO, 2023; AMINI et al., 2022; STNGANINI, 2023). However, few studies have explored free satellite images with high spatial resolutions in urban contexts. The CBERS-4A satellite has been used in several studies of land use and land cover (LULC) due to its spatial, spectral and temporal aspects. In particular, the WPM (Wide Scanning Multispectral and Panchromatic Camera) sensor aboard this satellite has high potential to be applied in various urban studies, including the mapping of impervious surfaces, due to its high spatial resolution of 2 m (INPE, 2022).

In addition to the satellite images, the use of machine learning algorithms have been proven to be very effective in various digital classifications in recent years, including those of urban areas (MARKERT et al., 2020; PAREKH et al., 2021). Examples of these methodologies include techniques such as Classification and Regression Trees (CARTs) (WANG et al., 2018; WANG et al., 2021), Random Forest (RF) (ZHENG et al., 2023; LIU; YANG; HUANG, 2023), Artificial Neural Networks (ANNs) (MAHYOUB et al., 2022) and Support Vector Machines (SVMs) (BROWN et al., 2022). By applying the RF to Landsat imagery using remote sensing techniques and innovative cloud services, Lodato et al. (2023) recorded the transformation of the coastal region in northern Rome, an important rural area, into new residential and commercial services. Dong et al. (2021) investigated the spatial and temporal variations of impervious surfaces on Beijing's sixth ring road using Landsat image data from 1997 to 2017 based on the RF method. The results showed an amount of 16.23% of improvement in classification accuracy for highly reflective impervious surfaces, revealing the effectiveness of RF in increasing the accuracy of impervious surface detection (DONG et al., 2021).

Investment in urbanization can benefit the general population. However, at the same time that this development occurs, the lack of planning is triggering socio-economic and environmental issues in cities throughout Brazil (TUCCI, 2008). In the city of Barreiras, as is the case of many Brazilian cities, the drainage systems are not enough to meet the high demand

for water caused by waterproofing and the vegetation cover suppression. In this context, this study aims to map the impermeable areas of the Barreiras city in western Bahia by integrating CBERS-4A fused images with the RF classifier.

2. Methodology

The study area is the urban perimeter of the Barreiras city, which is located in the western region of the Bahia state (Figure 1). This area covers ~ 8,051.274 km² (IBGE, 2021), with an average altitude of 452 m.

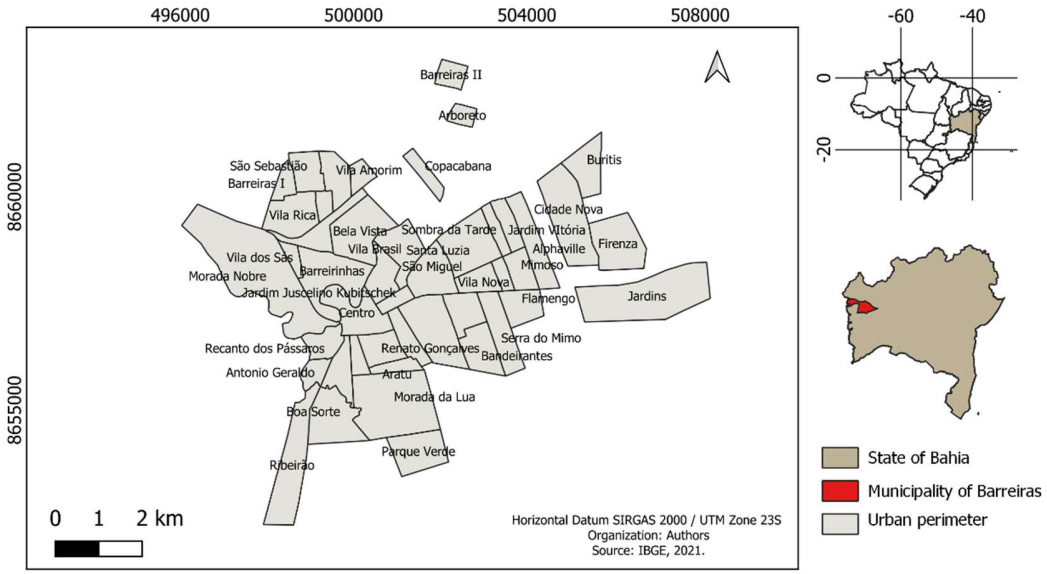

Figure 1 – Location of the urban perimeter of Barreiras, Bahia.
Source: Authors (2024).

According to the IBGE (2022), the population of Barreiras was of 137,000 in 2010, where 90% of this population lived in urban areas. The latest IBGE census (2022) in Brazil estimated that this city has a current population of 159,734 people and a population density of 19.84 inhabitants per square kilometer.

This study was carried out using images from the CBERS-4A / WPM sensor in the visible spectral range (B1 blue - 0.45 - 0.52 µm; B2 green - 0.52-0.59 µm; and B3 red - 0.63-0.69) and panchromatic (0.77- 0.89 µm). These images were download at the image generation division (DGI) of the National Institute for Space Research (INPE). The image dated 13/06/2023 was selected in this study as it showed less cloud cover and thus better radiometric quality to map the impermeable areas.

The blue, green and red bands (B1, B2 and B3) from the CBERS-4A satellite were merged using the merge/mosaic tool in the QGIS 3.28 software. Adjustments were made to the sharpness (equalization) of the merged image. After this step, the color of each layer was defined and some histogram adjustments were made to the image in order to improve the quality of the color composition.

In the multispectral mode, the CBERS-4A provides spectral bands with an average spatial resolution of 8 m, while in panchromatic mode they have a high spatial resolution of 2 m (INPE, 2023). The selected images were merged based on the QGIS using a procedure called Pansharpening, which consists of merging the multispectral and panchromatic images, making it possible to reduce the spatial resolution from 8 m to 2 m.

In this study, the digital image classification was performed based on the RF algorithm implemented in the Dzetsaka: Classification Tool package. The classes selected for classification were: vegetation, exposed soil, water, urban area and other (shadow from buildings). To carry out the classification, 100 samples were collected for each class, except for the class other, where an amount of 22 samples were collected. The RF classification method was used to generate the area percentages for each class. Basically, the RF grouped the decision trees and classified the pixels that fit the tree parameters. The parameters used in the RF classifier were those established as default in the Dzetsaka: Classification Tool package.

After classification, the Classification Report tool of the Semi-Automatic Classification Plugin was used to produce the percentage of each class in the Barreiras urban perimeter and subsequently, of each neighborhood. In this study, all types of built-up areas were assumed to be impermeable, considering that changes in the soil cover makes it less permeable, even if they are not completely removed. For the purposes of visual inspections with the classified image, fine spatial resolution Google Earth images were also used in this study.

As complementary data, we used a shapefile of the neighborhoods of the Barreiras urban perimeter based on the most recent zoning of the city's Master Plan, as well as the neighborhood boundary data available in Google Earth. The RF classification raster was clipped based on the limits of the neighborhoods to obtain the area value of each class in km² and the percentage of impermeable area per neighborhood. This allowed us to compare the percentage of waterproofing in each neighborhood, as well as to obtain the percentage in relation to the city's total perimeter.

Based on the RF classified image, the confusion matrix was generated and some accuracy metrics were calculated, including: the global accuracy, accuracy by class (producer and user) and the Kappa index (CONGALTON, 1991). The confusion matrix is a way of expressing the quality obtained from the classification of digital images, by analyzing validation samples together with the classification data (LILLESAND, T.; KIEFER, 1994; RICHARDS, 1993). Global accuracy, accuracy by class and the Kappa index were calculated using the Accuracy tool of the Semi-Automatic Classification Plugin (SCP) in QGIS, based on the equations 1 and 2:

$$F_m = \frac{\sum X_i}{N} * 100 \qquad \text{Equation 1}$$

$$k = \frac{N \sum_{i=1}^{r}(X_{ii}) - \sum_{i=1}^{r}(X_{i+}X_{+i})}{N^2 - \sum_{i=1}^{r}(X_{i+}X_{+i})} \qquad \text{Equation 2}$$

According to Congalton (1991):

k = Kappa coefficient;
N = Number of total observations (sample points);
r = Number of lines and columns of the confusion matrix;
X_{ii} = Number of observations in line i and column i;
X_{i+}= Total values of lines i;
X_{+i}= Total values of columns i.

The Kappa index ranges from -1 to 1. This index demonstrates the level of agreement of the data, generating indications of the accuracy of the classification results (LILLESAND, T.; KIEFER, 1994; RICHARDS, 1993). In addition, this index allows to compare different classification methods and results from previous classifications. In addition to the accuracy metrics, we also perform visual comparative analyses using high resolution images from Google Earth.

3. Results and discussion

Figure 2 shows the fused image from the CBERS-4A satellite and the samples (100) used to separate the impermeable areas in the classification. Preliminary visual inspections between the classified image and the complementary satellite images identified that the building shadow class was being wrongly classified as water, due to the proximity of their spectral signatures. For this reason, the building shadow class was included in this analysis in order to minimize classification errors. Further tests were also carried out before the final classification in order to identify possible problems of spectral confusion between the mapped classes.

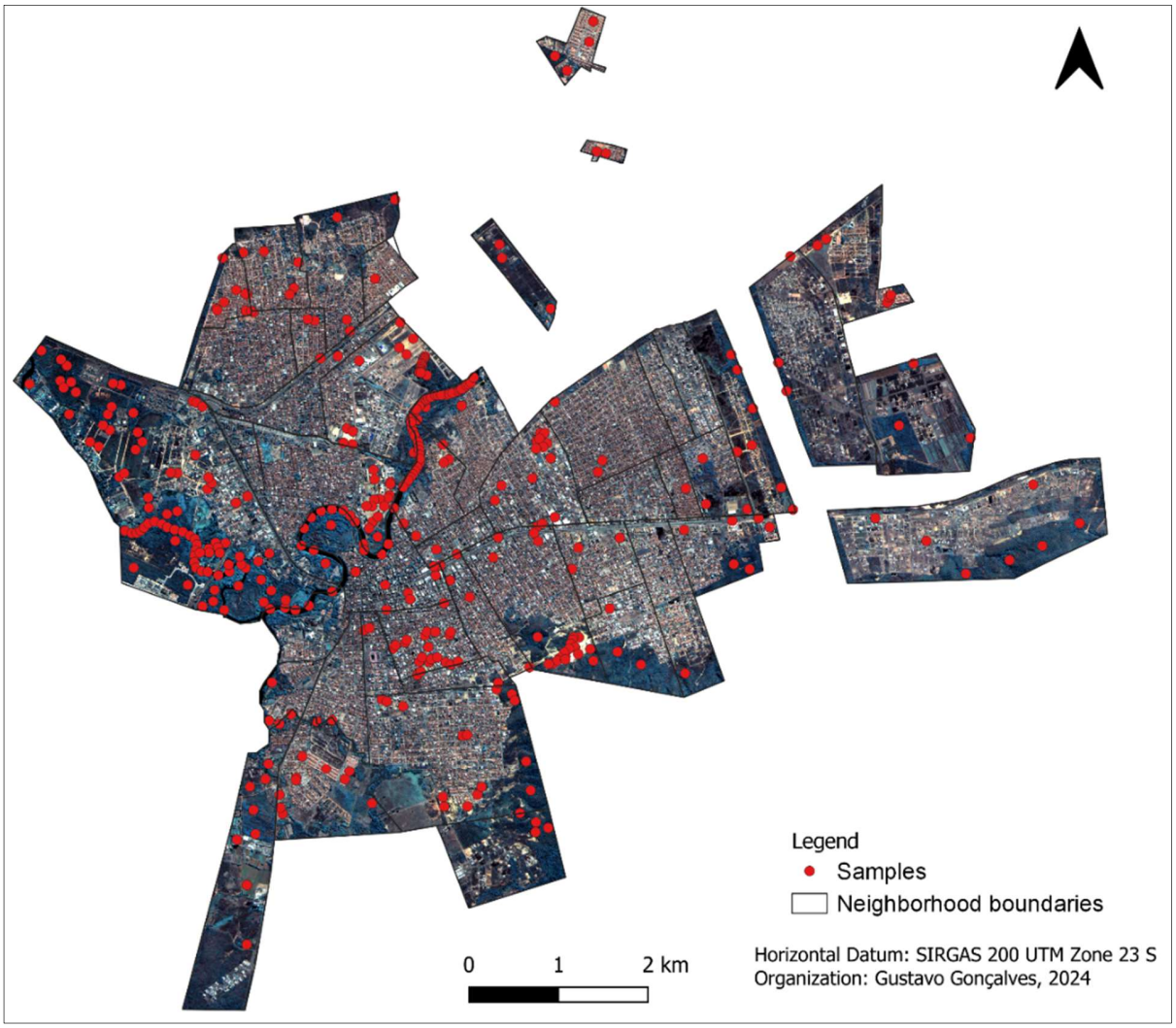

Figure 2 – CBERS-4A fused image highlighting the samples used to separate the impermeable areas. Source: Authors (2024).

Figure 3a-c illustrates the fused image, the Google Earth image and the classification by the RF (RF1) of a section of the Firenzi neighborhood, showing the classification errors due to confusion between the spectral responses of vegetation and exposed soil, and vegetation and urban area. In order to minimize these effects, one test was carried out to separate the more sparse vegetation from the urban area class. To do this, new samples were included and the sparse vegetation class was added. The results of this classification were not satisfactory, as confusion between pixels with sparse vegetation were still observed in some regions of the Barreiras urban perimeter.

Figure 3 – Example of image classification illustrating the confusion of vegetation pixels with urban areas. Source: Authors (2024).

One new classification test was performed (RF2), but now adding more samples, in order to separate the sparse vegetation class from the urban area, however, without success. In this test, pixels from urban areas were wrongly classified as pixels from sparse vegetation (Figure 4a-c).

Based on the results of the classification (RF2), we decided to follow the analyses with the results of the first classification (RF1) as it was visually more legitimate for the urban class, the focus of this study. The high spatial resolution panchromatic image (2 m) did not make it impossible to homogenize the pixels each other, since that the classified image maintained the 8 m spatial resolution of the multispectral images.

Figure 5a-c shows the targets with ceramic roofing material, where it is possible to identify the homogenization of the pixels (Figure 5a), which increases the difficulty of discriminating the roof of a house with ceramic tiles from exposed soil, due to their similar spectral responses.

One of the factors that makes it possible to collect the points and consequently make the classification more effective is the purity of the pixels. The urban area class, for example, is made up of different types of materials. The more diverse the arrangement of impermeable materials on the ground, the more possible it will be to mix up the pixels at this level of spatial resolution, impling in class confusion. This makes the RF classifier's performance difficult, as it receives very similar spectral responses with a resolution that does not help to divide the classes in detail. An alternative to minimize these effects would be to use higher spatial resolution images, such as those from Unmanned Aerial Vehicles (UAVs), for example. However, by imaging a smaller area on the ground, these images would not serve the purpose of analyzing the urban perimeter as a whole.

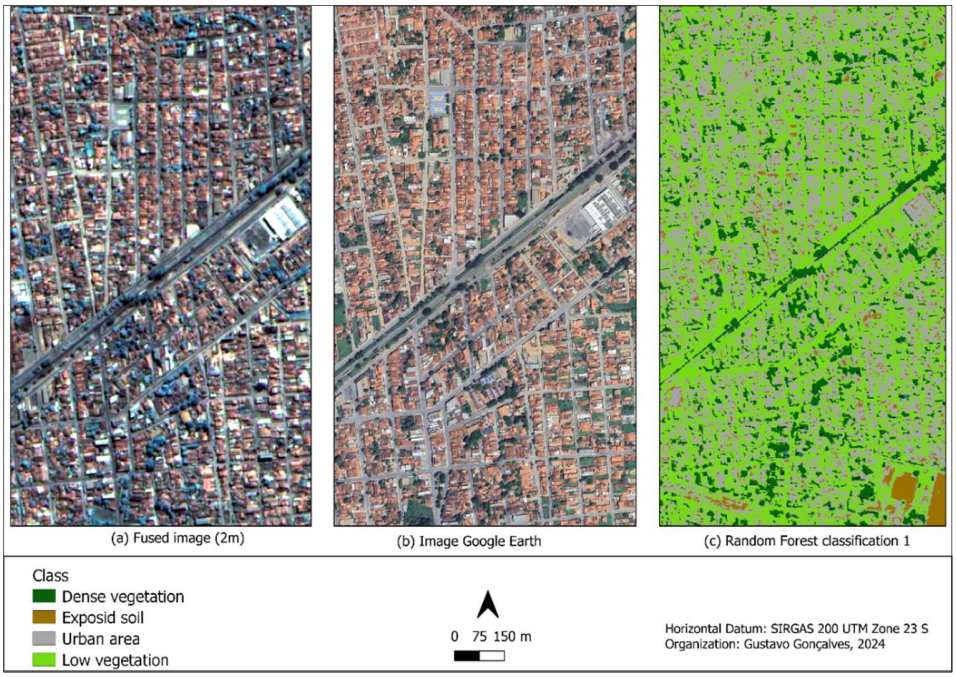

Figure 4 – Example of image classification illustrating the confusion of vegetation pixels with urban areas. Source: Authors (2024).

Figure 5 – Analysis of the ceramic roof in the Barreiras urban perimeter, BA. Source: Authors (2024).

Figure 6 shows another classification result, but now with a good visual agreement between the classified image and the high spatial resolution image from Google Earth (Figure 7). The result of this classification indicated a predominance of the vegetation class (18.54 km²), followed by the urban area (17.79 km²), exposed soil (6.41 km²) and water (0.44 km²) classes.

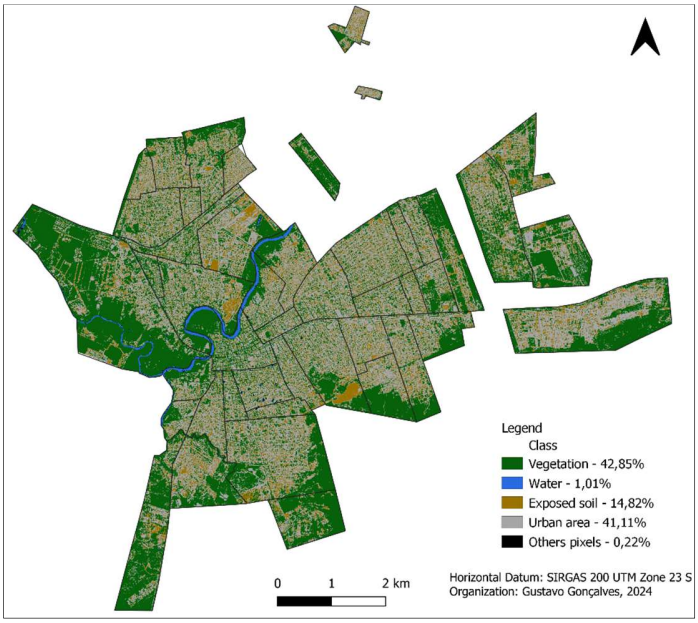

Figure 6 – Classification of the land use and land cover in Barreiras, BA, using the CBERS 4A image. Source: Authors (2024).

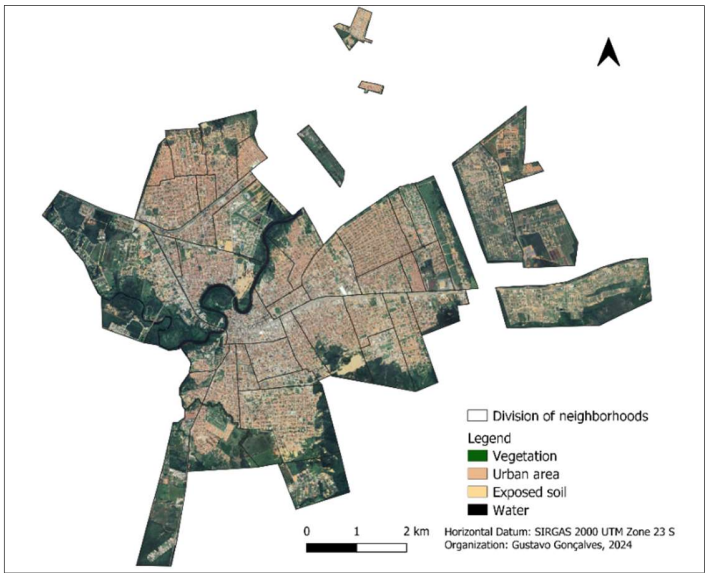

Figure 7 – Google Earth image of the city of Barreiras, BA. Source: Authors (2024).

The classification was evaluated based on the confusion matrix, overall accuracy, accuracy by class (producer and user accuracy) and the Kappa index. The results of the accuracy metrics are shown in Tables 1 and 2. The land use and land

cover map for the Barreiras urban perimeter revealed a high overall accuracy of 91.79%. The urban area class showed the greatest confusion of pixels with the other classes, as expected. From the total of 74,963 pixels for the matrix line, only 48,466 pixels were correctly classified as urban area, achieving 64.65% of accuracy. In the case of the exposed soil class, 20,533 pixels os this class were considered as urban area by the producer metric, which represents 27.39% of the total amount of the line, and confirms the confusion with urban elements. The vegetation class stood out with the largest number of classified pixels (305,169), obtaining the highest percentage of pixels correctly classified by the producer (300,560), representing 98.49% of agreement. In this class, the greatest confusion occurred with urban area, where 4,041 pixels were incorrectly classified.

Table 1 – Confusion matrix for the classes mapped in Barreiras, BA.

Class	Vegetation	Water	Exposed soil	Urban area	Others	Total
Vegetation	300560	27	0	5905	41	306533
Water	149	13627	0	36	347	14159
Exposed soil	247	0	8868	20533	0	29648
Urban area	4041	0	1519	48466	0	54026
Others	172	235	0	22	646	1075
Total	305169	13889	10387	74963	1034	405442

Source: Authors (2024).

Table 2 – Accuracy of the classification of land use and land cover in Barreiras, BA.

Class	Vegetation	Water	Exposed soil	Urban area	Others
User Accuracy %	98,05	96,24	29,91	89,71	60,09
Producer Accuracy %	98,49	98,11	85,38	64,65	62,48
Global Accuracy %	91,79				
Kappa Index by Class	0,92	0,96	0,28	0,87	0,60
Kappa Global	0,79				

Source: Authors (2024).

Accuracy by class (Table 2) showed the highest user accuracy values for the vegetation (98.05 %), water (96.24 %) and urban area (89.71 %) classes, while the lowest accuracies were found for the other (60.09 %) and exposed soil (29.91 %) classes. Similarly, the vegetation and water classes also showed the highest producer accuracy values, with 98.49 % and 98.11 %, respectively.

In this analysis, the urban area (64.65 %) and other (62.48 %) classes were the ones with the worst results. The greatest confusion of pixels occurred in the exposed soil with urban area (Table 1), where there is sparse vegetation with the presence of soil, observed in some neighborhoods of the Barreiras city that are still sparsely inhabited, usually on plots that have not yet been built on. The confusion between the water and the shadows of vertical buildings (other class - excluded pixels) is confirmed. In general, the classification showed satisfactory results according to the Kappa index, reaching an overall value of 0.79. The water class was the one with the highest Kappa index (0.96) and the exposed soil the class with the lowest value (0.28).

The confusion matrix confirms what has already been mentioned: the urban area, due to its diversity of materials, has impure pixels considering the spatial resolution of 2 m and thus, present more confusions with classes having similar spectral signatures. The spatial distribution of the total impermeable area was of 41.11% (Figure 8).

Figure 8 – Percentage of the total impermeable and non-permeable areas in the polygons of the neighborhoods of Barreiras, BA.
Source: Authors (2024)

Figure 9 shows the percentage (%) and the area (km²) of waterproofing in the Barreiras urban perimeter in relation to the area of each neighborhood. The neighborhoods with the highest area and percentage values were: Jardins, Morada Nobre and Cidade Nova, located in the northwest and northeast sectors of the Barreiras urban perimeter. On the other hand, the Jardim, Juscelino Kubitschek, Vila dos Funcionários and Copacabana neighborhoods, located in the north-central portion of the city's urban perimeter, showed the lowest values of waterproofing.

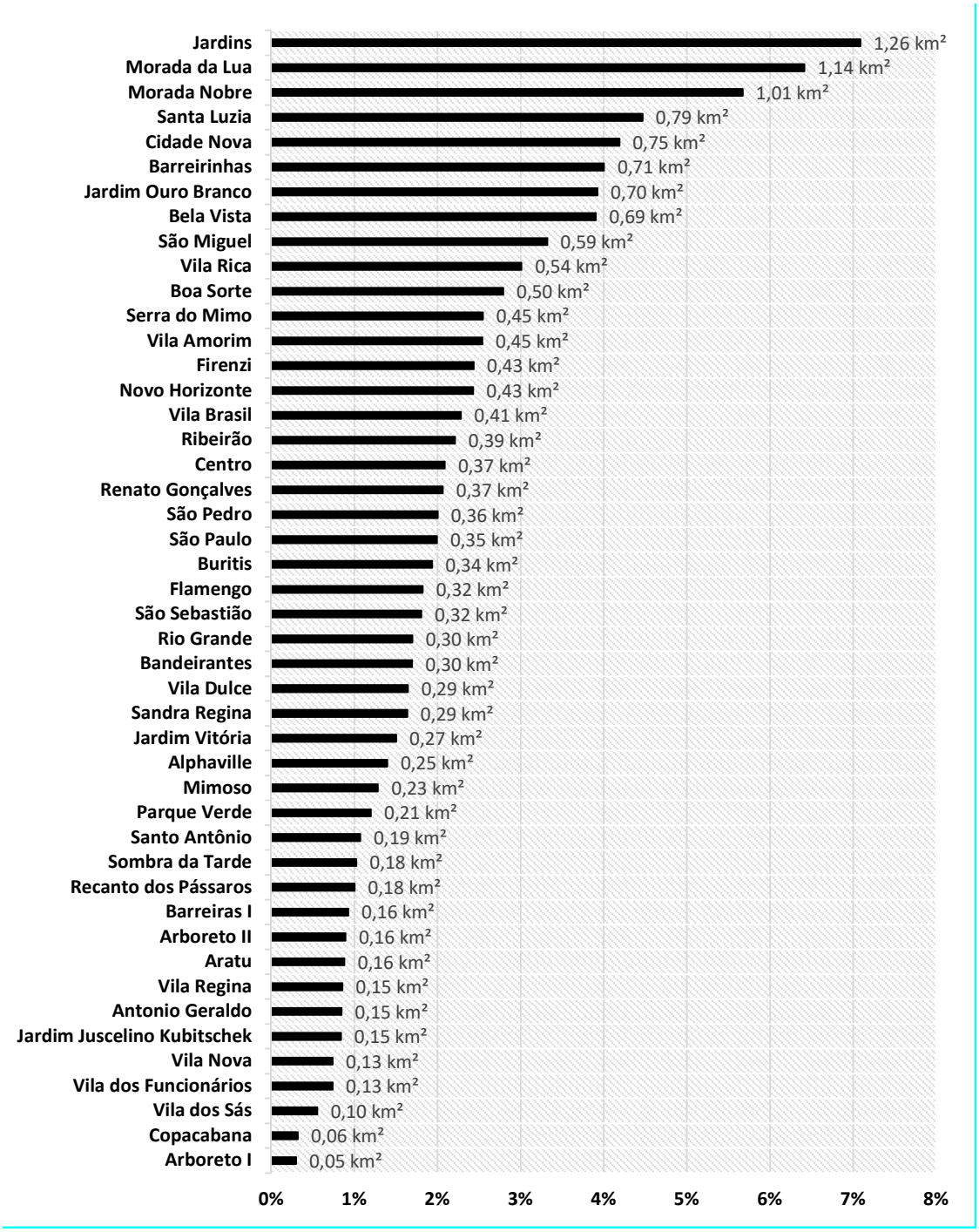

Figure 9 – Percentage (%) and area (km²) of waterproofing in the Barreiras urban perimeter in relation to the area of each neighborhood.
Source: Authors (2024).

As expected, some sparsely inhabited neighborhoods in the city of Barreiras had a high waterproofing percentage due to the large size of the neighborhood and the fact that much of it is composed by sparse vegetation. As an example, the

Jardins neighborhood (Figure 10) is at the top of the classification (Figure 9), with the highest concentration of urban densification compared to the other neighborhoods. It is also possible to see large open areas composed by vegetation and exposed soil.

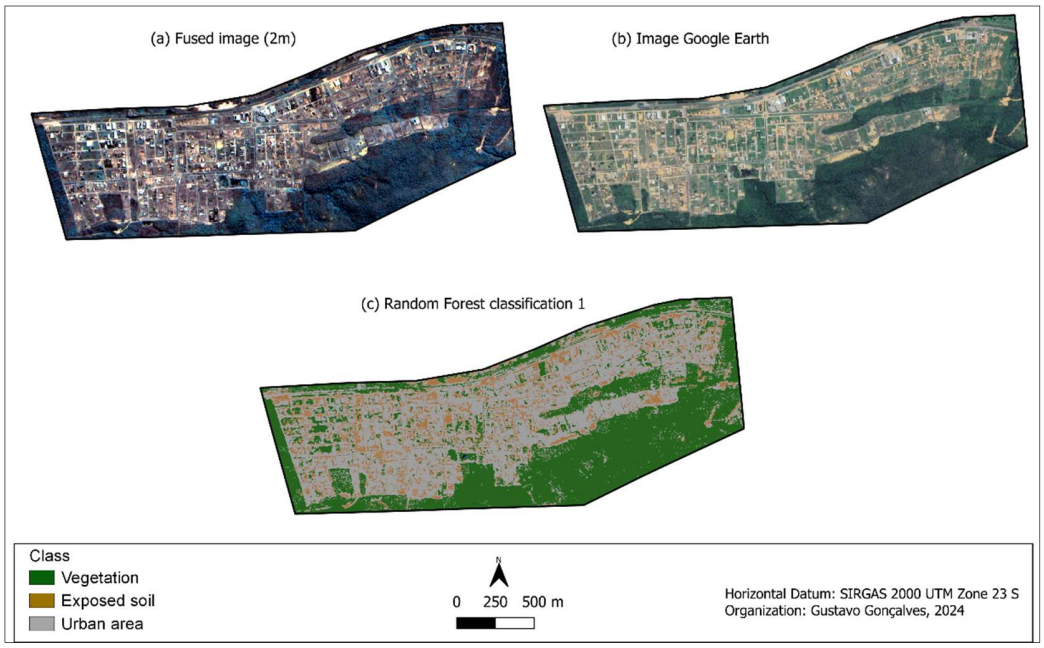

Figure 10 – Comparative analysis between the fused image, Google Earth and classified image for the Jardins neighborhood in Barreiras, BA.
Source: Authors (2024).

Similarly, other neighborhoods with great confusion between classes, but which revealed a high percentage of waterproofing, include Cidade Nova (Figure 11), showing some pixel confusion, predominantly with exposed soil and urban area to the north of this neighborhood. It is also possible to see a confusion of sparse vegetation and urban areas in the neighborhood's roundabouts in the main road that crosses the neighborhood diagonally.

The Morada Nobre (Figure 12), Morada da Lua (Figure 13) and Santa Luzia (Figure 14) neighborhoods showed the best results in the classification, while the Jardins (Figure 10) and Cidade Nova (Figure 11) neighborhoods stood out with great confusion in the classes. The Morada da Lua neighborhood showed a waterproofing index of 6.41% of the total, agreeing with the merged CBERS - 4A image and the high-resolution Google Earth image, where a large part of this neighborhood is composed by built-up area. The Santa Luzia neighborhood has the smallest spatial extent compared to the other neighborhoods, however, it is the most populous in the city (PREFEITURA DE BARREIRAS, 2019). This neighborhood is dominated by roads and houses, representing 4.47% in relation to the percentage of the entire Barreiras urban perimeter.

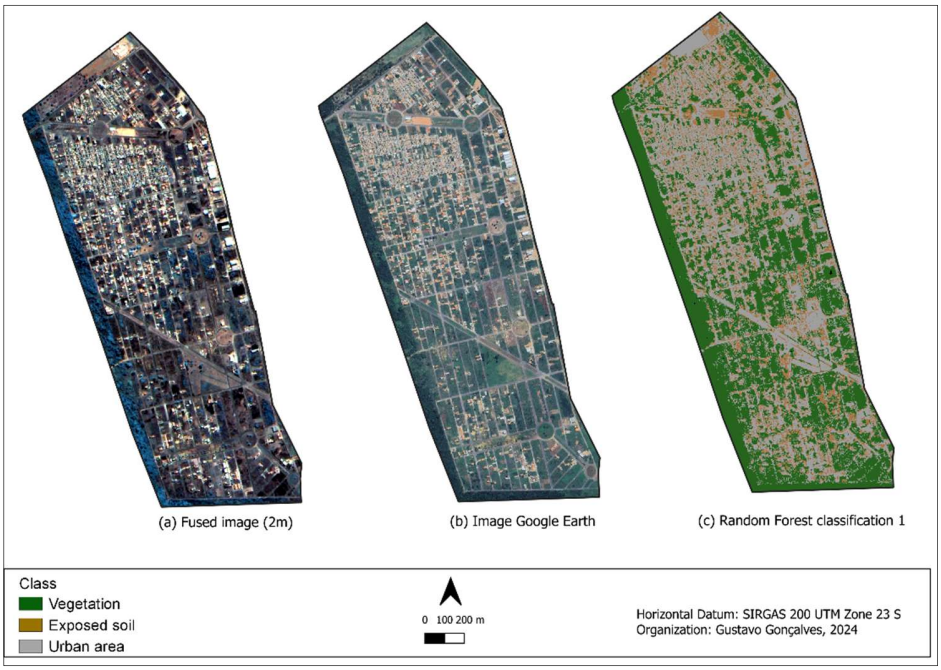

Figure 11 – Comparative analysis between the fused image, Google Earth image and classified image for the Cidade Nova neighborhood in Barreiras, BA.
Source: Authors (2024).

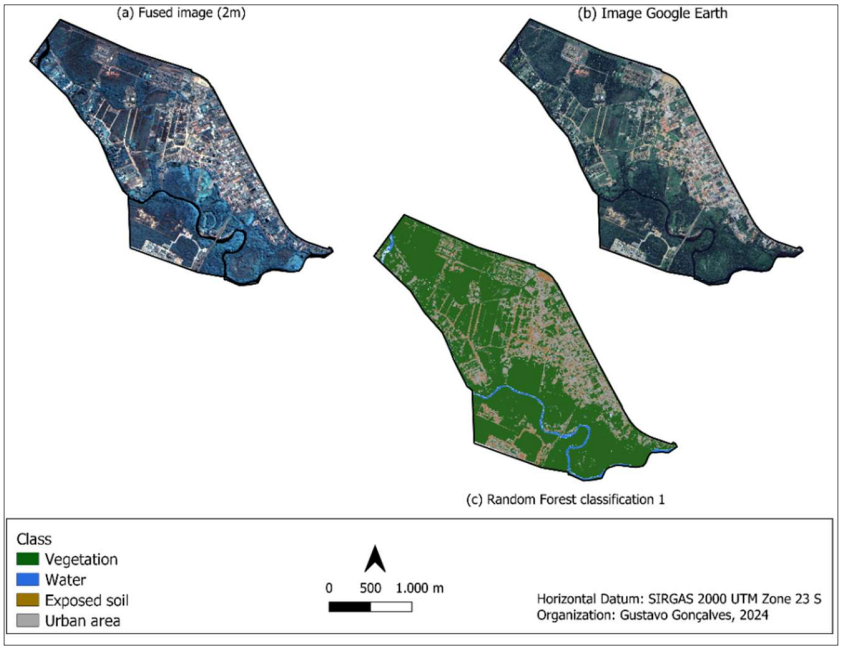

Figure 12 – Comparative analysis between the fused, classified and Google Earth images for the Morada Nobre neighborhood in Barreiras, BA.
Source: Authors (2024).

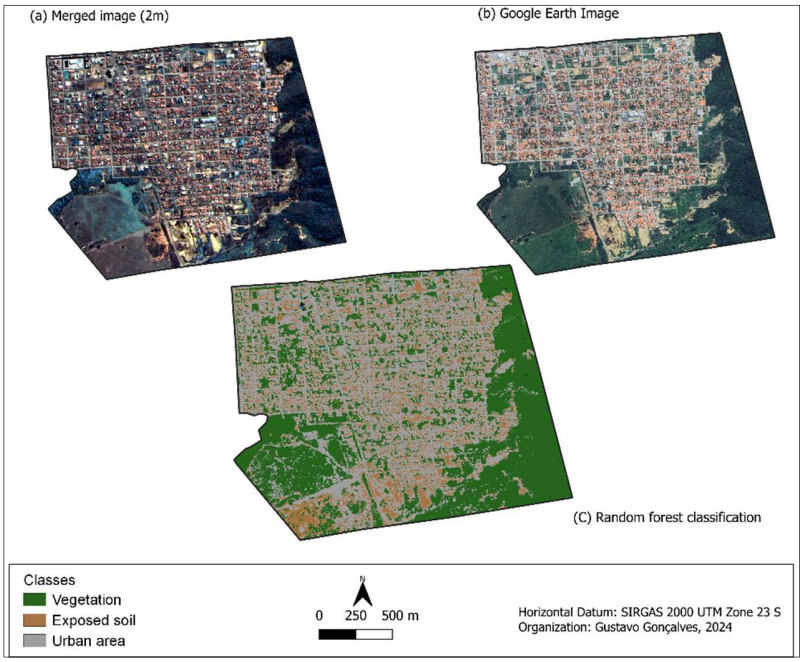

Figure 13 – Comparative analysis between the fused, classified and Google Earth images for the Morada da Lua neighborhood in Barreiras, BA. Source: Authors (2024).

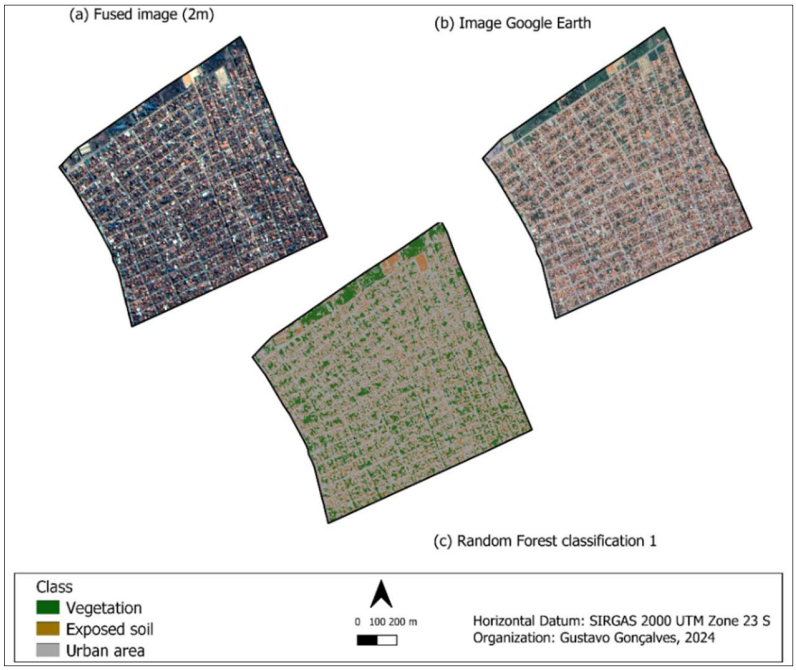

Figure 14 – Comparative analysis between the fused, classified and Google Earth image for the Santa Luzia neighborhood in Barreiras, BA.
Source: Authors (2024).

The confusions found between impermeable and sparse vegetation areas, as well as exposed soil with ceramic roof, are explained by the similar spectral signatures of the materials involved in the classification. In the case of sparse vegetation, which was confused with gray tons in the fused image, it is possible that this result had occurred naturally. Maybe this vegetation was dry or this type of vegetation may have been grow in an area composed by organic soil. In this case, the shade is closer to black. However, it cannot be ruled out that the sun angle at the time the image was taken by the satellite may have influenced the shading of this vegetation, when compared with the Google Earth image, for instance.

The results found here show that the city of Barreiras has 41.11% of impermeable surfaces. Among the neighborhoods, Morada da Lua, Morada Nobre and Santa Luzia showed the highest percentages of impermeable surfaces, with 6.41%, 5.67% and 4.47%, respectively.

The difference in the spectral behavior of the different types of materials present in the urban land cover means that the classification shows similarities in the spectral analysis of the impermeable area at the 2m spatial resolution used in this study. In this way, the different types of materials (asphalt, concrete, fiber cement, ceramic and zinc tiles) may overestimate or underestimate some classified areas.

Dong et al. (2021) used the Random Forest (RF) algorithm in Beijing to study the spatio-temporal changes of impervious surfaces from Landsat satellite images. The accuracy assessment of this study showed that the classification strategy, combining spectral and textural features, performs optimally in complex urban areas, achieving a Kappa coefficient of 0.85. The results obtained by Dong et al. (2021) corroborate those found here, in which a Kappa index of 0.79 and an overall accuracy of 91.79% were obtained. Wu; Pan (2023) analyzed impervious surfaces in the urban area of Nachang, China, using CBERS-4A, Landsat 8 and Sentinel-1 images. The authors used the RF algorithm and obtained global accuracy results ranging from 88.3% to 92.55%. Previous studies, with similar applications of spatio-temporal analysis of impervious surfaces in urban areas, have presented similar results to those obtained here, including Hirye et al. (2015), Sun et al. (2017), Chang et al. (2020), Sobieraj; Fernández; Metelski (2022).

4. Final Remarks

This study showed the potential of: CBERS-4A images fused with the high spatial resolution band (2m); and the RF algorithm (involving random selection of features and random selection of samples) for mapping impermeable surfaces in urban areas. The results allowed us to quantify the percentage and area (km²) of waterproofing covering the entire Barreiras urban perimeter in Western Bahia, and relating it to the area of each neighborhood. Our findings fill a gap in the city's urban planning by providing new data.

The classification showed satisfactory accuracy metrics, specially the global accuracy and the Kappa index. The water and exposed soil classes, analyzed individually, had the highest and lowest accuracy values, respectively. The response of these metrics complemented the visual agreement found between the classified image and the Google Earth image. The user accuracy and producer accuracy metrics revealed errors of omission and commission in the mapped classes. In this sense, the neighborhoods with the highest density of impermeable areas showed low pixel confusions in the classes.

The heterogeneity of the urban targets was presumably differentiated by the high resolution spectral band, but resulted in similar classification responses. The different types of materials (asphalt, concrete, fiber cement, ceramic and zinc tiles) may have overestimated or underestimated some classified areas.

The results found here can elucidate the technical-scientific bases in the state of the art for future research into land use and land cover mapping of impermeable surfaces in urban settings using remote sensing/machine learning techniques and high spatial resolution bands.

References

Amini S., Saber, M. Rabiei–Dastjerdi, H., Homyouni, S. Urban Land Use and Land Cover Change Analysis Using Random Forest Classification of Landsat Time Series. Remote Sensing, 14, 11, 2654, 2022. https://doi.org/10.3390/rs14112654.

Belgiu, M., Drăgu, L. Random Forest in remote sensing: A review of applications and future directions. ISPRS J. Photogramm. Remote Sensing, 114, 24–31, 2016.

Cai, B., Shao, Z., Fang, S., Huang, X., Tang, Y., Zheng, M., Zhang, H. The Evolution of Urban Agglomerations in China and How It Deviates from Zipf's Law. Geo–spatial Information Science, 27, 1, pp. 38–48, 2022. https://doi.org/10.1080/10095020.2022.2083527.

Chang, S., Wang, Z.; Mao, D., Guan, K.; Jia, M., Chen, C. Mapping the Essential Urban Land Use in Changchun by Applying Random Forest and Multi–Source Geospatial Data. Remote Sensing, *12,* 15, 2488, 2020 https://doi.org/10.3390/rs12152488.

Dong, X., Meng, Z., Wang, Y., Zhang, Y., Sun, H., Wang, Q. Monitoring Spatiotemporal Changes of Impervious Surfaces in Beijing City Using Random Forest Algorithm and Textural Features. Remote Sensing, 13, 153, 2021. https://doi.org/10.3390/ rs13010153.

Hirye, M. C. de M., Alves, D., Kux, H. Mapeamento da cobertura da terra na cidade de Altamira (PA) em 2000 e 2010, com a utilização do modelo linear de mistura espectral de imagens do sensor TM. Revista Brasileira de Cartografia, 67, 1, 157–168, 2015. DOI: https://doi.org/10.14393/rbcv67n1–44731 .

IBGE. Instituto Brasileiro de Geografia e Estatística. *Censo Demográfico 2022*. Disponível em: https://www.ibge.gov.br/estatisticas/sociais/populacao/22827–censo–demografico–2022.html?edicao=35938&t=resultados/. Acesso em: 1/05/2023.

IBGE. Instituto Brasileiro de Geografia e Estatística. *População Rural e Urbana*. Disponível em: https://educa.ibge.gov.br/%20jovens/conheca–o–brasil/populacao/18313–populacao–rural–e–urbana.html . Acesso em: 08/06/2023.

INPE. Instituto Nacional de Pesquisas Espaciais. Câmeras Imageadoras CBERS 04A. Disponível em: http://www.cbers.inpe.br/sobre/cameras/cbers04a.php. Acesso em: 22/04/2023.

Kotarba, A.Z., Aleksandrowicz, S. Impervious surface detection with nighttime photography from the International Space Station. Remote Sensing of Environment, 176, 295–307, 2016. https://doi.org/10.1016/j.rse.2016.02.009.

Kuang, W., Hou, Y., Dou, Y., Lu, D., Yang, S. Mapping Global Urban Impervious Surface and Green Space Fractions Using Google Earth Engine. Remote Sensing 13, 4187, 2021. https://doi.org/10.3390/rs13204187

Li, W., Wu, C., & Zang, S. Modeling urban land use conversion of Daqing City, China: a comparative analysis of "top–down" and "bottom–up" approaches. Stochastic Environmental Research and Risk Assessment, 28, 4, 817–828, 2014. http://dx.doi.org/10.1007/s00477–012–0671–0.

Li, Wenliang. Mapping Urban Impervious Surfaces by Using Spectral Mixture Analysis and Spectral Indices. *Remote Sensing, 12,* 1, 94, 2020. https://doi.org/10.3390/rs12010094.

Lillesand, T., Kiefer, R.W. *Remote Sensing and Image Interpretation.* 3.ed. New York: John Wiley & Sons, 1994, 768p.

Liu, Z., Yang, J., Huang, X. Landsat–Derived Impervious Surface Area Expansion in the Arctic from 1985 to 2021. Sci. Total Environ. 905, 166966, 2023. https://doi.org/10.1016/j.scitotenv.2023.166966.

Mahyoub, S., Rhinane, H., Mansour, M., Fadil, A., Okaishi, W.A. Impervious Surface Prediction in Marrakech City Using Artificial Neural Network. International Journal of Advanced Computer Science and Applications IJACSA., 13, 185–189, 2022. https://doi.org/10.1016/j.scitotenv.2023.166966.

Markert, K.N., Markert, A.M., Mayer, T., Nauman, C., Haag, A., Poortinga, A., Bhandari, B.; Thwal, N.S., Kunlamai, T., Chishtie, F., et al. Comparing sentinel–1 surface water mapping algorithms and radiometric terrain correction processing in southeast asia utilizing google earth engine. Remote Sensing. 12, 2469, 2020. https://doi.org/10.3390/rs12152469.

Naikoo, M. W., Rihan, M., Ishtiaque, M., Shahfahad. Analyses of land use land cover (LULC) change and built–up expansion in the suburb of a metropolitan city: Spatio temporal analysis of Delhi NCR using landsat datasets. Journal of Urban Management, 9, 3, 347–359, 2020. https://doi.org/10.1016/j.jum.2020.05.004.

Njoku, E. A., Tenenbaum, D. E. Aquantitative assessment of the relationship between land use/land cover (LULC), topographic elevation and land surface temperature (LST) in Ilorin, Nigeria. Remote Sensing Applications: Society and Environment, 27, 100780, 2022. https://doi.org/10.1016/j.rsase.2022.100780.

Olivatto, T. F., Inguaggiato, F. F., Stanganini, F. N. Urban mapping and impacts assessment in a Brazilian irregular settlement using UAV–based imaging. Remote Sensing Applications: Society and Environment, 29, 100911, 2023. https://doi.org/10.1016/j.rsase.2022.100911.

Parekh, J.R., Poortinga, A., Bhandari, B., Mayer, T., Saah, D. Chishtie, F. Automatic Detection of Impervious Surfaces from Remotely Sensed Data Using Deep Learning. Remote Sensing, 13, 16, 3166, 2021. https:// doi.org/10.3390/rs13163166

PREFEITURA DE BARREIRAS. *Relatório Plano Diretor – Planejamento Participativo*: Barreiras, 2019.

Richards, J. A. *Remote Sensing Digital Image Analyses*: an introduction. 2. ed. Berlin: Springer–Verlag, 1993, 340p.

Saah, D., Tenneson, K., Matin, M., Uddin, K., Cutter, P., Poortinga, A., Nguyen, Q. H., Patterson, M., Johnson, G., Markert, K., et al. Land cover mapping in data scarce environments: Challenges and opportunities. Frontiers in Environmental Science, 7, 150, 2019. https://doi.org/10.3389/fenvs.2019.00150.

Shao, Z.; Cheng, T.; Fu, H.; Li, D.; Huang, X. Emerging Issues in Mapping Urban Impervious Surfaces Using High–Resolution Remote Sensing Images. Remote Sensing, 15, 2562, 2023. https://doi.org/10.3390/ rs1510256.

Sobieraj, J.; Fernández, M.; Metelski, D. A. Comparison of Different Machine Learning Algorithms in the Classification of Impervious Surfaces: Case Study of the Housing Estate Fort Bema in Warsaw (Poland). Buildings, 12, 12, 2115, 2022. https://doi.org/10.3390/buildings12122115.

Su, S., Tian, J., Dong, X., Tian, Q., Wang, N., Xi, Y. An Impervious Surface Spectral Index on Multispectral Imagery Using Visible and Near–Infrared Bands. Remote Sensing, 14, 14, 3391, 2022. https://doi.org/10.3390/rs14143391.

Sun, Z., Wang, C., Guo, H., Shang, R. A Modified Normalized Difference Impervious Surface Index (MNDISI) for Automatic Urban Mapping from Landsat Imagery. *Remote Sensing, 9*, 9, 942, 2017; https://doi.org/10.3390/rs9090942.

Tucci, C.E.M. (2008). Águas urbanas. Estudos avançados, 22, 63, 97–112.

UNO. United Nations Organization. (2018). *World Urbanization Prospects: The 2018 Revision*. UN Department of Economic and Social Affairs: New York, NY, USA, 2018.

Wang, J.; Wu, Z.; Wu, C.; Cao, Z.; Fan, W.; Tarolli, P. Improving Impervious Surface Estimation: An Integrated Method of Classification and Regression Trees (CART) and Linear Spectral Mixture Analysis (LSMA) Based on Error Analysis. Gisci. Remote Sensing, 55, 4, 583–603, 2018. https://doi.org/10.1080/15481603.2017.1417690.

Wang, Y., Huang, Q., Zhao, A., Lv, H., Zhuang, S. Semantic Network–Based Impervious Surface Extraction Method for Rural Urban Fringe from High Spatial Resolution Remote Sensing Images. IEEE J. Sel. Top. Applied Earth Observations and Remote Sensing, 14, 4980–4998, 2021. http://dx.doi.org/10.1109/JSTARS.2021.3078483.

Wu, Y. Pan, J. Detecting Changes in Impervious Surfaces Using Multi–Sensor Satellite Imagery and Machine Learning Methodology in a Metropolitan Area. Remote Sensing, 15, 22, 5387, 2023. https://doi.org/10.3390/rs15225387.

Zhang, L, Yugang Tian, Y., Liu, Q. A Novel Urban Composition Index Based on Water–Impervious Surface–Pervious Surface (W–I–P) Model for Urban Compositions Mapping Using Landsat Imagery. Remote Sens. 13, 1, 3, 2021. https://dx.doi.org/10.3390/rs13010003.

Zheng, Z., Yang, B., Liu, S.; Xia, J. Zhang, X. Extraction of Impervious Surface with Landsat Based on Machine Learning in Chengdu Urban, China. Remote Sensing Applications: Society and Environment, 30, 100974, 2023. https://doi.org/10.1016/j.rsase.2023.100974.

Zhu, Z., Qiu, S.; Ye, S. Remote Sensing of Land Change: A Multifaceted Perspective. Remote Sensing of Environment 282, 1, 113266, 2022. https://doi.org/10.1016/j.rse.2022.113266.